Received: 21 September 2021 | Revised: 22 December 2021 | Accepted: 28 December 2021

DOI: 10.1111/cas.15269

ORIGINAL ARTICLE

Cancer Science WILEY

HSP90 promotes radioresistance of cervical cancer cells via reducing FBXO6-mediated CD147 polyubiquitination

Qi Song[1] | Juyi Wen[2] | Weiping Li[1] | Janxin Xue[3] | Yufei Zhang[4] | Hongyan Liu[4] | Jixia Han[4] | Tao Ning[5] | Zejun Lu[2]

[1]Senior Department of Obstetrics and Gynecology, the Seventh Medical Center of PLA General Hospital, Beijing, China

[2]Oncology Department, the Sixth Medical Center of PLA General Hospital, Beijing, China

[3]Department of Thoracic Oncology, Cancer Center and State Key Laboratory of Biotherapy, West China Hospital, Sichuan University, Chengdu, China

[4]Senior Department of Oncology, the Fifth Medical Center of PLA General Hospital, Beijing, China

[5]Tianjin Medical University Cancer Institute and Hospital, Tianjin, China

Correspondence
Zejun Lu, Oncology Department, the Sixth Medical Center of PLA General Hospital, Beijing, China.
Email: lzjpla@126.com

Abstract

HSP90 inhibition might be a promising strategy to overcome the radioresistance of some cancers. In the current study, we further explored the mechanisms of HSP90 in regulating the radiosensitivity of cervical cancer cells. Bioinformatic analysis was performed based on data from TCGA-CESC. Cellular and molecular studies were conducted using CaSki and SiHa and the derived radioresistant (RR) subclones. Through a proteomics screen, we identified HSP90 chaperones (both HSP90α and HSP90β) as CD147-binding partners supporting its stabilization. Targeting HSP90 sensitized CaSki-RR and SiHa-RR cancer cells to irradiation partially through CD147 destabilization. Mechanistically, HSP90 interacts with FBXO6 and reduces FBXO6-mediated proteasomal degradation of CD147. Enforced *FBXO6* overexpression also sensitized CaSki-RR and SiHa-RR cancer cells to irradiation. These effects were enhanced using 17-AAG treatment but were weakened by *CD147* overexpression. Survival analysis further confirmed the association between high *FBXO6* expression and favorable progression-free survival among patients with cervical cancer. In conclusion, this study showed that HSP90 promotes radioresistance of cervical cancer cells partially via reducing FBXO6 mediated CD147 polyubiquitination. These findings help to explain why HSP90 inhibitor exerts radio-sensitizing effects in cervical cancer.

KEYWORDS
CD147, cervical cancer, FBXO6, HSP90, radiotherapy

1 | INTRODUCTION

Cervical cancer is a leading cause of cancer death in women worldwide.[1] During the past decades, the application of new risk-screening techniques, such as The ThinPrep cytologic test (TCT), human papillomavirus (HPV) DNA detection, and high-risk HPV E6/E7 mRNA detection help to detect premalignant dysplasia and cervical cancer in the early stages in developed countries.[2] The growing vaccination coverage also makes cervical cancer preventable. However, in low- and middle-income countries, many patients are diagnosed in advanced stages with limited therapeutic options.[3]

Currently, radiation therapy remains an essential component for cervical cancer to achieve a cure.[4] In the definitive setting, chemoradiation is recommended for stages IB3-IVA, and radiotherapy or chemoradiation is conditionally recommended for stages IA1-IB2 when medically inoperable.[4] In addition, brachytherapy is strongly

recommended for all cases receiving definitive radiotherapy.[4] However, clinical outcome was heavily hampered by radioresistance,[5,6] the underlying mechanisms of which remain to be disclosed.

Heatshock protein 90 (HSP90) is a group of inducible ATP-dependent molecular chaperones in response to cellular stress. Four isoforms of HSP90 have been identified in mammalian cells, including Hsp90α (encoded by *HSP90AA1*) and Hsp90β (*HSP90AB1*) in the cytosol, Grp94 in the endoplasmic reticulum, and Trap1 in mitochondria.[7] Unlike the small HSPs (such as HS40s and HSP70s), which primarily support the degradation of irreversibly damaged proteins and reduce aggregation of misfolded proteins, HSP90 mainly enhances the stability and function of conformationally labile proteins after primary folding.[8] Hsp90α and Hsp90β are highly homologous, with 85% sequence identity.[9] Therefore, these 2 proteins share similar activities in regulating client proteins.[10] A series of HSP90 client proteins is involved in oncogenic processes, such as receptor tyrosine kinases (vascular endothelial growth factor receptor [VEGFR], epidermal growth factor receptor [EGFR], and rb-b2 receptor tyrosine kinase 2 [ERBB2]), transcription factors (HIF-1α, BCL6, and OCT4), apoptosis-associated proteins (BCL2 and BIRC5), cell cycle regulatory proteins (Cyclin D1, CDK4, and WEE1) and signal transduction proteins (AKT, NF-κB, B-RAF, and c-MET).[7,8] Therefore, HSP90 inhibition has been considered as a high-potential strategy for cancer therapy. Several HSP90 inhibitors have been developed for animal studies or have entered clinical trials for various refractory cancers, such as SNX-7081, GDA, STA-9090, SNX-2112, and 17-AAG, a synthetic analog of geldanamycin.[7]

Previous studies have observed that HSP90 inhibition might be a promising strategy to overcome radioresistance of some cancer cells, such as lung cancer cells,[11] soft tissue sarcoma cells,[12] pancreatic cancer,[13] and cervical cancer.[14,15] In the current study, we further explored the mechanisms of HSP90 in regulating the radiosensitivity of cervical cancer.

2 | MATERIALS AND METHODS

2.1 | Bioinformatic analysis

The expression profile of HSP90AA1 and HSP90AB1 in patients with primary cervical cancer and their association with survival outcomes, including progression-free survival (PFS) and overall survival (OS) were analyzed based on data extracted from The Cancer Genome Atlas Cervical Squamous Cell Carcinoma and Endocervical Adenocarcinoma (TCGA-CESC), using the UCSC Xena Browser.[16] Kaplan-Meier survival curves were generated between patients with the top 25% and bottom 25% of gene expression.

2.2 | Gene set enrichment analysis (GSEA)

GSEA was conducted using software 4.1.0 from the Broad Institute. Patients with primary CESC in TCGA-CESC were separated into 2 groups by median *HSP90AA1* or *HSP90AB1* expression. Then, single-gene GSEA was conducted within the Hallmark gene sets. Gene set permutations were set to 1000 to obtain a normalized enrichment score (NES). Only the gene sets with NES >1, Nominal (NOM) $P < .05$, and a false discovery rate (FDR) q-value <0.25 were compared.

2.3 | Cell culture and treatment

Cervical cancer cell lines CaSki and SiHa were obtained from the American Type Culture Collection (ATCC, Manassas, VA, USA) and were cultured following the method introduced previously.[17] X-ray resistant sublines (CaSki-RR and SiHa-RR) were generated following the strategy described previously.[18] In brief, cells were cultured in 25-cm^2 culture flasks and were irradiated with a 2 Gy dose at a rate of 1.2 Gy/min using an RS 2000 Xray Irradiator (160 kV, 25 mA, 0.3 mm copper filters) (Rad Source Tech, Suwanee, GA, USA). When cells reached ~80% confluency, the cells were cultured in new dishes. When they reached ~50% confluency, they were irradiated again. The irradiation (IR) cycles were stopped when the total dose reached 60 Gy. Cells were allowed to recover for 2 wk before further experiments.

Lentiviral *CD147* shRNAs were generated based on the pLKO.1-EGFP-puro plasmid, with the following shRNA sequence: #1, 5′-CCAGAATGACAAAGGCAAGAA-3′; #2, 5′-GCTACACATTGAGAACCTGAA-3′. Lentiviral particles carrying *CD147* (NM_001728) with flag-tag, wild-type FBXO6 (NM_018438, FBXO6-WT) or mutant FBXO6 (p.Y241A and p.W242A, FBXO6-MT) were generated based on the pLV-IRES-GFP-puro plasmid. Cells were infected with lentivirus at an MOI of 10. Cells were infected with harvested lentivirus for 48 h for transient infection. Cells with stable gene expression or knockdown were selected using 2 μg/mL puromycin for 1 wk. MG132 (a typical proteasome inhibitor), tanespimycin (17-AAG) and cycloheximide (CHX) (a protein synthesis inhibitor) were purchased from Sigma-Aldrich (Saint Louis, MO, USA). 17-AAG treatment was performed depending on experimental readouts.

2.4 | Western blotting and immunoprecipitation (IP)

Total protein from cellular samples was extracted using a cold radioimmunoprecipitation assay lysis buffer (RIPA) buffer (20 mM Tris [pH7.5], 150 mM NaCl, 1% Triton X-100, sodium pyrophosphate, β-glycerophosphate, EDTA, Na_3VO_4, leupeptin and protease inhibitors) (P0013, Beyotime, Shanghai, China) buffer. The cell lysates were cleared by centrifugation at 100 000 × ***g*** for 30 min at 4°C to generate the soluble samples. Then, protein concentration was quantified using a BCA Protein Assay Kit (Beyotime). RIPA-insoluble pellets were then extracted with urea buffer (7 M urea, 2 M thiourea, 4% CHAPS, 30 mM Tris, pH 8.5 + protease inhibitors). Then, the

samples were centrifuged at 100 000 × ***g*** for 30 min at 22°C. Next, 20 μg of protein samples were loaded into each lane of an SDS-PAGE gel, separated using electrophoresis, and then transferred to nitrocellulose (NC) membranes (Merck Millipore, Burlington, MA, USA). After blocking with 5% BSA, the membranes were incubated with primary antibodies and corresponding secondary antibodies. The protein bands were developed using BeyoECL Star chemiluminescence reagents (Beyotime).

An IP assay was conducted using the Pierce Co-Immunoprecipitation Kit (ThermoFisher Scientific), and following the manufacturer's instruction. For each co-IP assay, 10 μg antibody was used. The eluted samples were subjected to western blotting.

The primary antibodies using included rabbit anti-HSP90α (1:1:1000, PA3-013, ThermoFisher Scientific) and rabbit anti-HSP90β (1:1:1000, PA3-012, ThermoFisher Scientific), mouse anti-FBXO6 (sc-134339, Santa Cruz Biotechnology, Dallas, TX, USA), mouse anti-CD147 (1:5000, 66443-1-Ig, Proteintech, Wuhan, China), rabbit anti-γ-H2AX (1:1000, ab2893, Abcam, Cambridge, USA) and mouse anti-β-actin (1:5000, 66009-1-Ig, Proteintech).

2.5 | Liquid chromatography-tandem mass spectrometry (LC-MS/MS)

LC-MS/MS assay was conducted to analyze the protein samples immunoprecipitated by anti-HSP90α or anti-HSP90β, following the strategy introduced in 1 previous study.[19]

2.6 | Quantitative real-time reverse transcription-PCR (qRT-PCR) analysis

Total RNA was extracted from cellular samples using TRIzol reagent (Invitrogen, Carlsbad, CA, USA) was then reversely transcribed into cDNA using the PrimeScript RT Kit (Takara, Dalian, Liaoning, China). qRT-PCR was performed using a SYBR Green kit (Takara). β-Actin mRNA was used as a reference gene for normalization. Relative gene expression was calculated using the $2^{-\Delta\Delta Ct}$ method. Primer sequences are listed in Table S1.

2.7 | Clonogenic assay

Cells were seeded into 24-well plates and were irradiated at defined doses (0, 2, 4, 6, or 8 Gy) after adhesion, using a RS 2000 Xray Irradiator. After 14 d of incubation, cells were washed, fixed with methanol, and stained with 0.1% crystal violet. Colonies containing >50 cells were counted using microscope inspection. The plating efficiency (PE) of un-irradiated cells (0 Gy) was calculated by the formula: PE = number of colonies counted/number of cells plated. Surviving fraction (SF) of the irradiated cells was calculated using the formula: SF = number of colonies formed after treatment/number of cells seeded × PE. A linear-quadratic model was utilized to generate survival curves using the following equation[20]: $Y = \exp(-1 \times (A \times X + B \times X^2))$, in which Y is the fraction survival and X is the dose. A equals −1 times the initial slope, and the initial value of B equals −0.1 times the initial slope.

2.8 | Mice and treatment

Animal procedures were approved by the Institutional Animal Care and Use Committee (IACUC) of the Fifth Medical Center of PLA General Hospital, Beijing, China. Nude mice (BALB/c-nude, 5-wk-old females) were purchased from Vital River Laboratories (Beijing, China). Mice were randomly assigned into 6 groups. Here, 2×10^6 cells (CaSki-RR, SiHa-RR, and the cell lines with stable *CD147* knockdown or overexpression) suspended in a 1:1 mixture of culture medium and Matrigel Matrix (Corning, Glendale, AZ, USA) were subcutaneously injected into the lower back. For 17-AAG treatment groups, 17-AAG was administered 50 mg kg^{-1} for 5 times per wk via ip injection after xenograft reached ~100 mm^3. For IR treatment groups, mice were anesthetized with 2% isoflurane before partial body IR and shielded with lead. Only tumors were then irradiated using the RS 2000 Xray Irradiator (Rad Source) irradiation source. A total dose of 20 or 30 Gy (10 Gy/every 8 d) X-ray radiation was given, at a dose rate of 1.2 Gy/min. Tumor size was measured every 4 d using calipers . Tumor volume (V) was calculated with the following formula: $V = AB^2/2$, in which A is the long axis diameter and B is the short axis diameter. When tumor volume reached ~1000 mm^3 in the largest tumor group mice were sacrificed. Tumors were removed, photographed, and sectioned. Tumor proliferation was determined using Ki-67 immunohistochemistry (IHC) staining, while tumor cell apoptosis was assessed using terminal transferase-mediated dUTP nick end labeling (TUNEL) staining.

2.9 | Immunohistochemistry (IHC) staining

Commercial human cervical cancer tissue arrays were purchased from Taibosi Biotechnology (Xian, China). IHC staining was performed with a Leica BOND-III, automatic IHC and ISH Stainer (Leica, Wetzlar, Germany). The following antibodies were used, including anti-HSP90α (1:50, PA3-013, ThermoFisher Scientific, Carlsbad, CA, USA), anti-HSP90β (1:50, 37-9400, ThermoFisher Scientific) and anti-Ki-67 (1:2000, 27309-1-AP, Proteintech). Protein expression scores were conducted by 2 experienced pathologists without authorship in this study, according to the criteria proposed by the Human Protein Atlas. In brief, the score is a combination and conversation of staining intensity and fraction of stained cells. Four staining scores were defined, including not detect, low, medium, and high (https://www.proteinatlas.org/about/help#4).[21]

2.10 | Immunofluorescence assay

The level of phosphorylated histone variant H2AX (γ-H2AX), which is a surrogate marker of DNA damage is detected using immunofluorescence assay. In brief, CaSki-RR and SiHa-RR cells with *FBXO6* overexpression alone or together with *CD147* overexpression were plated onto culture slides (Corning Inc, Corning, NY, USA). When cells reached ~50% of confluence, cells were subjected to 17-AAG (20 nM/24 h for CaSki-RR and 50 nM/24 h for SiHa-RR) or control pre-treatment and then treated with 2 Gy irradiation. At 6 h later, the cells were fixed with buffered formaldehyde for 15 min and then permeabilized with 0.02% Triton. The cells were then blocked in 3% albumin in Dulbecco's phosphate-buffered saline (DPBS) for 1 h. Then, the slides were incubated with a primary antibody against γ-H2AX (AP0687, ABclonal, Wuhan, China) in a 1:200 dilution in the 3% albumin solution overnight at 4°C. Then, the slides were thoroughly washed and incubated with goat anti-rabbit IgG (H&L) (Alexa Fluor 647) (ab150079, Abcam, Cambridge, UK) secondary antibody in a 1:500 concentration in albumin. The slides were kept in darkness for 1 h before washing. The slides were mounted using VECTASHIELD Antifade Mounting Medium with 4', 6-diamidino-2-phenylindole (DAPI). Then, fluorescence images were captured using an FV1000 confocal laser scanning biological microscope (Olympus, Tokyo, Japan).

2.11 | Statistical analysis

Statistical analysis was performed using GraphPad Prism 8.1.2. Quantitative data were reported as mean ±standard deviation (SD). Statistical analysis of the statistical difference between 2 groups was estimated based on the unpaired *t* test with Welch correction. One-way ANOVA with Tukey's post hoc multiple-comparisons testing was performed. The difference between the survival curves was estimated by Log-rank (Mantel-Cox) test. *P*-values of .05 or less were determined as statistically significant. * and #, $P < .05$; ** and ##, $P < .01$; *** and ###, $P < .001$.

3 | RESULTS

3.1 | *HSP90AA1* and *HSP90AB1* upregulation was associated with poor survival of patients with cervical cancer

With RNA-seq data acquired from GTEx-fallopian tube (FT) ($n = 5$), GTEx-cervix ($n = 13$), and primary cervical cancer tissues from TCGA ($n = 304$), we examined the expression profile of *HSP90AA1* and *HSP90AB1*. Results showed that *HSP90AA1* expression was significantly upregulated in the tumor group compared with normal tissue groups (Figure 1A, left). In comparison, no significant alteration of *HSP90AB1* mRNA expression was observed among these groups (Figure 1A, right). Then, K-M survival analysis was performed between the primary tumor cases with the top 25% and bottom 25% of *HSP90AA1* and *HSP90AB1* expression. Patients with the top quartile of *HSP90AA1* expression had substantially shorter PFS, compared with the counterparts with the bottom quartile of gene expression (Figure 1B). However, no significant difference was observed in OS between the 2 groups (Figure 1C). High *HSP90AB1* expression was associated with significantly shorter PFS and OS, compared with the counterparts with the bottom quartile of gene expression (Figure 1D,E). IHC staining showed that among 20 cases of cervical tumor tissues examined, 13/20 and 12/20 cases had medium to high level of HSP90α and HSP90β expression, respectively (Figure 1F-H).

To understand the functional role of HSP90 in cervical cancer, we conducted a GSEA assay between patients with high and low *HSP90AA1* or *HSP90AB1* expression in TCGA-CESC (Table S2 and S3). GSEA identified that the gene set of DNA repair was associated with higher *HSP90AA1* or *HSP90AB1* expression (bold front, Figure S1). As tumor cells with a strong DNA repair capacity are usually radioresistant[22] and HSP90 inhibitor has been considered a promising radio-sensitizer,[23] we decided to explore the underlying mechanisms. Radioresistant CaSki (CaSki-RR) and SiHa (SiHa-RR) cells were generated (Figure S2A-C). These 2 subclones had significantly elevated HSP90 expression at both mRNA and protein levels (Figure S2D,E).

3.2 | HSP90 binds to and stabilizes CD147 in radioresistant cervical cancer cells

To explore the regulatory mechanisms of HSP90 in cervical cancer, we explored their interacting proteins via sequential use of IP, SDS-PAGE, and LC-MS/MS. By cross-comparing the candidates with the potential interactors of HSP90α/β in BioGRID (https://thebiogrid.org/), we found that CD147 and FBXO6 are 2 high-potential candidates (Figure 2A). Co-IP assays confirmed the interaction among HSP90α/HSP90β, CD147, and FBXO6 in CaSki-RR (Figure 2B-D) and SiHa-RR (Figure 2E-G) cells. In CaSki-RR and SiHa-RR cells, CD147 expression was significantly upregulated at the protein level, but not the mRNA level, compared with parental cell lines (Figure S2F). As FBXO6 acts as a substrate recognition component of the Skp1-Cullin1-F-box protein (SCF) ubiquitin E3 ligase complex,[24] we decided to explore the functional significance of the bindings in terms of CD147 protein stability. 17-AAG was applied to treat CaSki-RR and SiHa-RR cells. Interestingly, treatment with 17-AAG reduced total CD147 protein levels in a dose-dependent manner (Figure 2H,I). Then, CaSki-RR and SiHa-RR cell lysates were separated into RIPA-soluble and RIPA-insoluble urea parts. 17-AAG treatment reduced CD147 protein levels in both soluble and insoluble samples (Figure S3A) but did not alter *CD147* mRNA expression (Figure S3B). Therefore, these findings implied that HSP90 interacts with and stabilizes CD147 in cervical cancer cells.

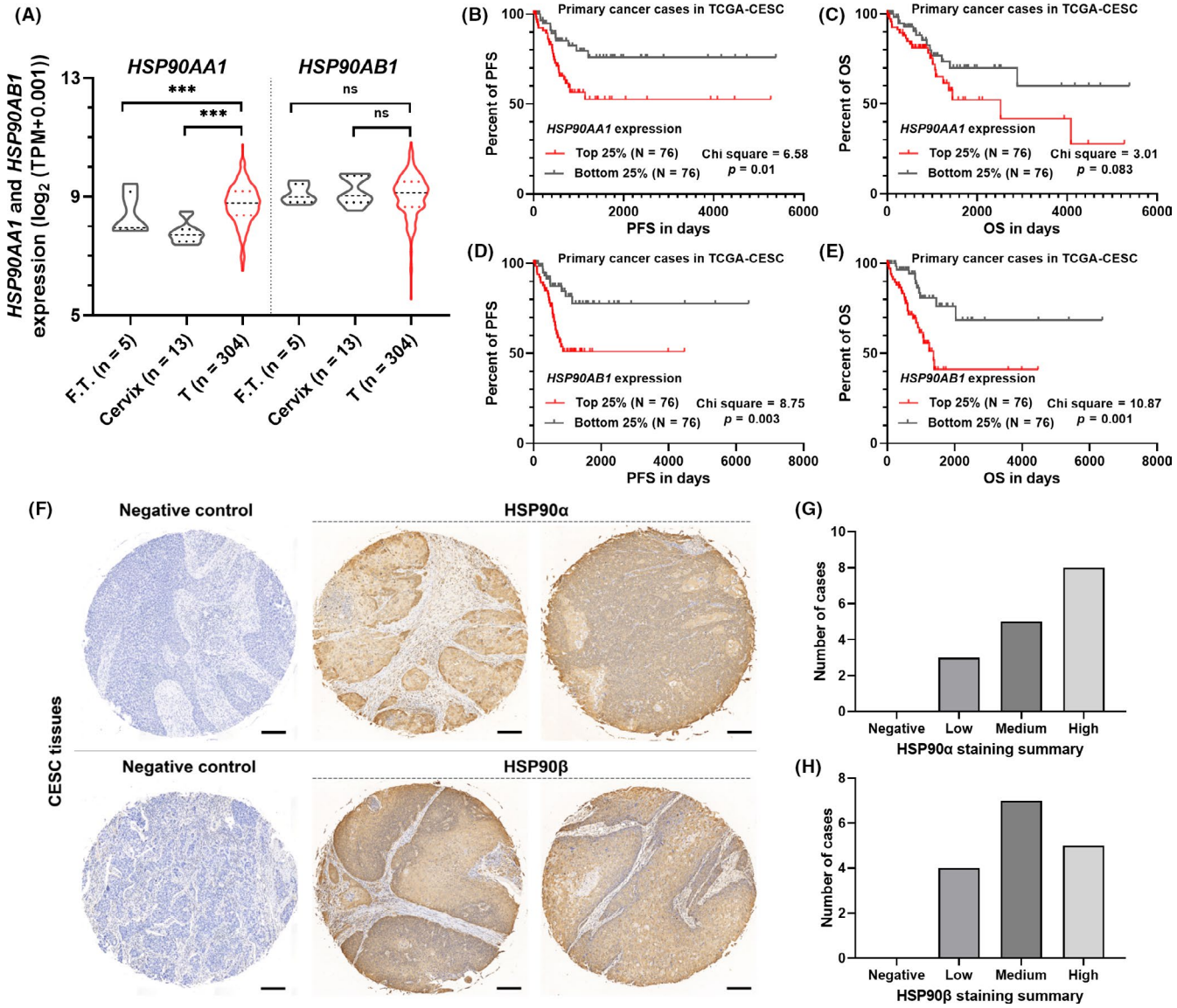

FIGURE 1 *HSP90AA1* and *HSP90AB1* upregulation is associated with poor survival of patients with cervical cancer. A, *HSP90AA1* and *HSP90AB1* expression profile in GTEx-fallopian tube (FT) ($n = 5$), GTEx-cervix ($n = 13$) and primary cervical cancer tissues from TCGA ($n = 304$). B-E, K-M survival analysis was performed to compare the difference in PFS (B, D) and OS (C, E) between primary cervical cancer cases with the top 25% and bottom 25% of *HSP90AA1* (B, C) and *HSP90AB1* (D, E) expression. F-H, Representative IHC images of HSP90α and HSP90β staining (F) and quantitation of IHC results in 20 cases of cervical cancer tissues (G, H)

3.3 | Inhibition of HSP90 sensitizes radioresistant cervical cancer cells to radiotherapy partially via CD147

Previous studies have shown that HSP90 inhibition might be a promising strategy to overcome radioresistance in multiple cancers,[11,14] but the mechanisms were still not fully understood. As HSP90 can stabilize CD147 in cervical cancer cells, we explored whether CD147 expression contributed to radioresistance. CaSki and SiHa cells were transiently infected lentivirus carrying *CD147* shRNA (Figure S4A,C,D) or flag-CD147 (Figure S4B,E). Cells with *CD147* knockdown had reduced colony formation when exposed to X-ray IR (Figure S4F,G). In contrast, cells with *CD147* overexpression had enhanced colony formation after IR (Figure S4H,I).

Similar experiments were performed using CaSki-RR and SiHa-RR cells. These RR cells with stable *CD147* knockdown (Figure 3A,C) exhibited reduced colony formation when exposed to X-ray IR (Figure 3E,F). In comparison, cells with *CD147* overexpression (Figure 3B,D) exhibited enhanced colony formation after IR and were less responsive to 17-AAG (Figure 3G,H). In vivo assays showed that *CD147* knockdown alone significantly reduced the growth of CaSki-RR and SiHa-RR cell-derived tumors and also enhanced IR-induced growth suppression (Figure 3I-K). *CD147* overexpression reduced the radio-sensitizing effect of 17-AAG (Figure 3I-K). Immunofluorescence TUNEL staining and

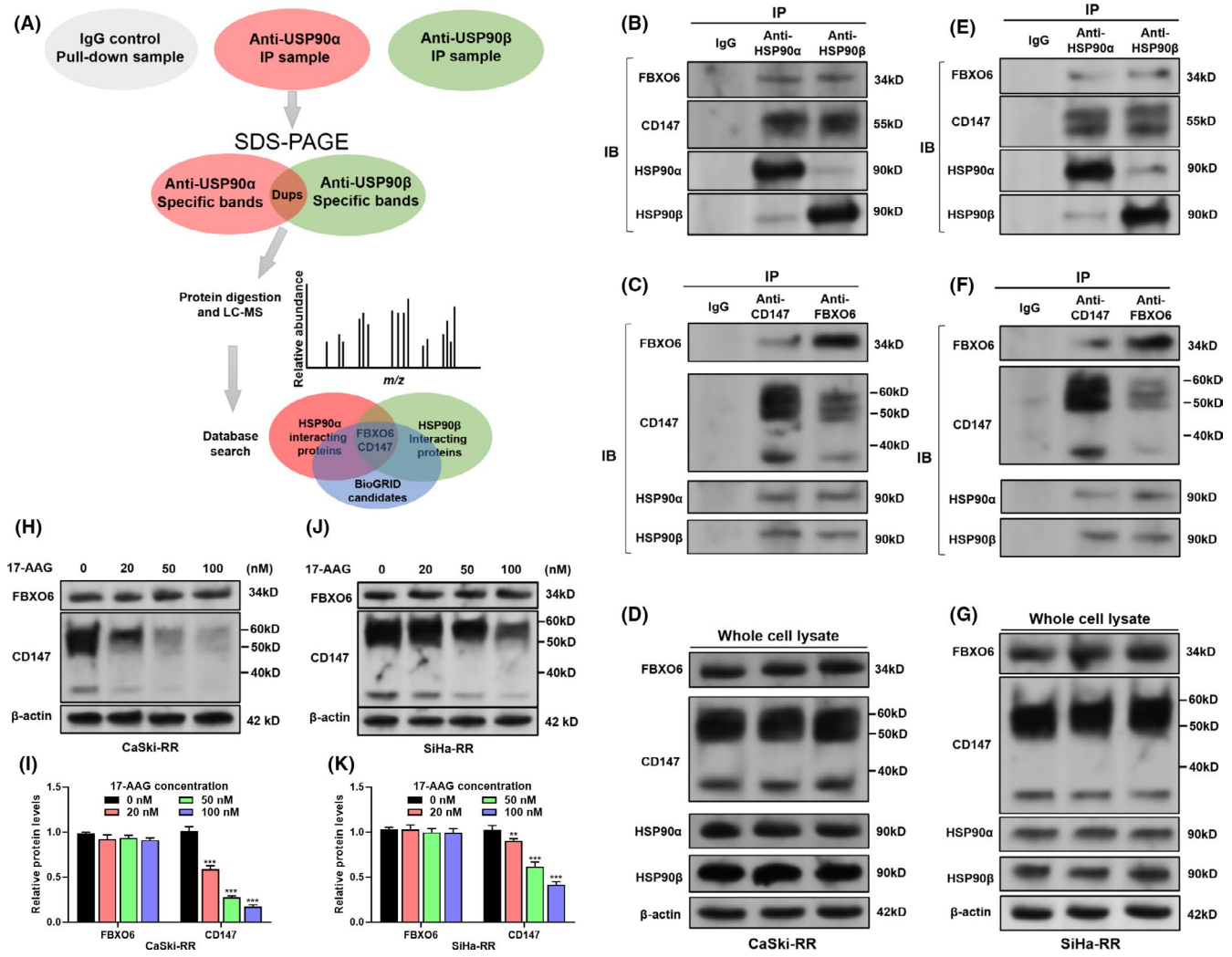

FIGURE 2 HSP90 binds to and stabilizes CD147 in radioresistant cervical cancer cells. A, Workflow chart showing the process to identify proteins interacting with both HSP90α and HSP90β. FBXO6 and CD147 were identified as 2 potential candidates. B-G, Co-IP assays were conducted using anti-HSP90α and anti-HSP90β (B, E), or anti-CD147 and FBXO6 (C, F) in the lysates from CaSki-RR (B, C) and SiHa-RR (E, F) cells. Whole-cell lysates of CaSki-RR (D) and SiHa-RR (G) cells were used as positive controls. H-K, Representative images (H, J) and quantitation (I, K) of the effect of HSP90 inhibition on FBXO6 and CD147 protein levels. CaSki-RR (H, I) and SiHa-RR (J, K) cells were treated with increasing concentrations of 17-AAG for 24 h. FBXO6 and CD147 protein levels were determined by western blotting. Data are representative of 3 independent biological experiments. Data are reported as the mean ±SD from 3 technical replicates

IHC staining of Ki-67 revealed a higher level of TUNEL-positive cells, but a lower level of Ki-67-positive cells in *CD147* knockdown and 17-AAG treatment groups compared with the IR alone group (Figure 3L). However, *CD147* overexpression partly weakened the synergistic effect of 17-AAG and IR on inducing cell apoptosis (Figure 3L).

3.4 | Inhibition of HSP90 enhances the polyubiquitination of CD147 that leads to proteasomal degradation

To understand the molecular mechanisms through which HSP90 stabilizes CD147 in radioresistant cervical cancer cells, we checked the protein levels of CD147 influenced by 17-AAG, with or without the presence of MG132. Results showed that treatment with MG132 prevented 17-AAG associated flag-CD147 degradation in both CaSki and SiHa cells (Figure 4A,B) and reduced endogenous CD147 degradation in both CaSki-RR and SiHa-RR cells (Figure 4C,D). Treatment with 17-AAG enhanced flag-CD147 polyubiquitination (Figure 4E,F). Treatment with MG132 led to accumulated CD147 polyubiquitination, which was further enhanced by HSP90 inhibition (Figure 4G,H). CHX chase assay confirmed that 17-AAG treatment significantly facilitated CD147 degradation in both CaSki-RR and SiHa-RR cells (Figure 4I-L). These results suggested that CD147 was more susceptible to ubiquitin-mediated proteasomal degradation when HSP90 is functionally inhibited.

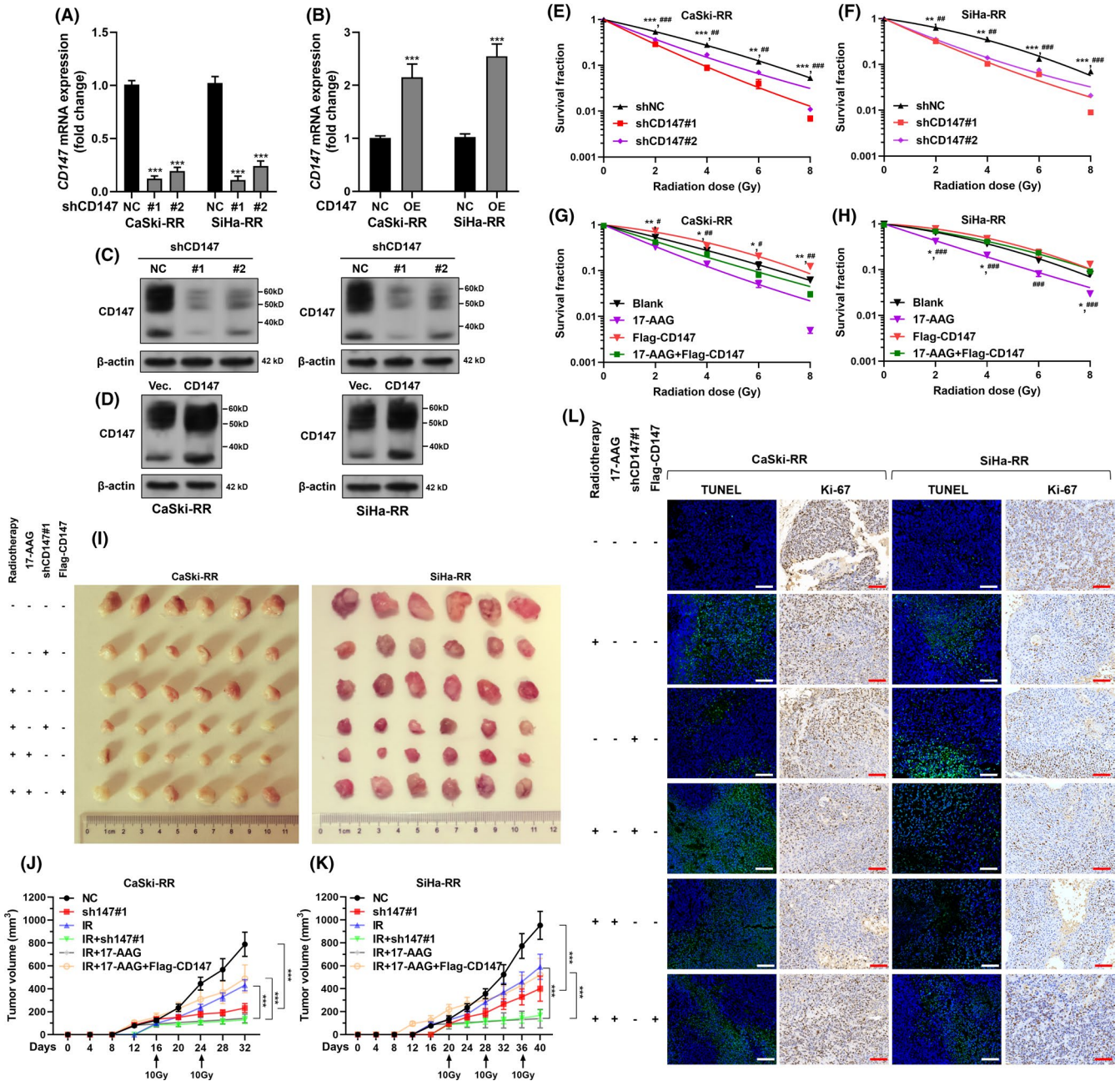

FIGURE 3 Inhibition of HSP90 sensitizes radioresistant cervical cancer cells to radiotherapy partially via CD147. A-D, qRT-PCR (A, B) and western blotting assay (C, D) to detect *CD147* expression at the mRNA and protein levels in CaSki-RR and SiHa-RR cells with stable *CD147* knockdown (A, C) or overexpression (B, D). E-H, Quantitation of clonogenic assay to examine the effects of X-ray IR (0, 2, 4, 6, and 8 Gy) on cell growth of CaSki-RR and SiHa-RR cells with *CD147* knockdown (E, F) or *CD147* overexpression alone or combined with 17-AAG treatment (20 nM/24 h for CaSki-RR and 50 nM/24 h for SiHa-RR) (G, H). *, Comparison between shNC and shCD147#1, and between blank and flag-CD147. #, Comparison between shNC and shCD147#2, and between 17-AAG and 17-AAG+flag-CD147. I-K, Representative images (I) tumor volume curves (J, K) of CaSki-RR and SiHa-RR cell-derived xenografts in nude mice receiving indicating treatments. L, Representative images of TUNEL staining and IHC staining of Ki-67 in tumor sections from panel (I)

3.5 | FBXO6 ubiquitinates and degrades CD147

As endogenous protein interactions among FBXO6, HSP90, and CD147 were confirmed by co-IP in both CaSki-RR and SiHa cells (Figure 2B-F), we then explored whether FBXO6 was involved in CD147 degradation. *FBXO6* overexpression reduced the CD147 protein levels and, conversely, knockout of FBXO6 led to elevated CD147 protein levels in CaSki-RR and SiHa cells (Figure 5A-D). However, FBXO6 modulation did not alter the protein expression of HSP90 (Figure 5A,C), suggesting that the effect of FBXO6 on CD147 was specific. Then, we conducted CHX chase assays to check the degradation of CD147 by FBXO6 modulation. *FBXO6* knockdown

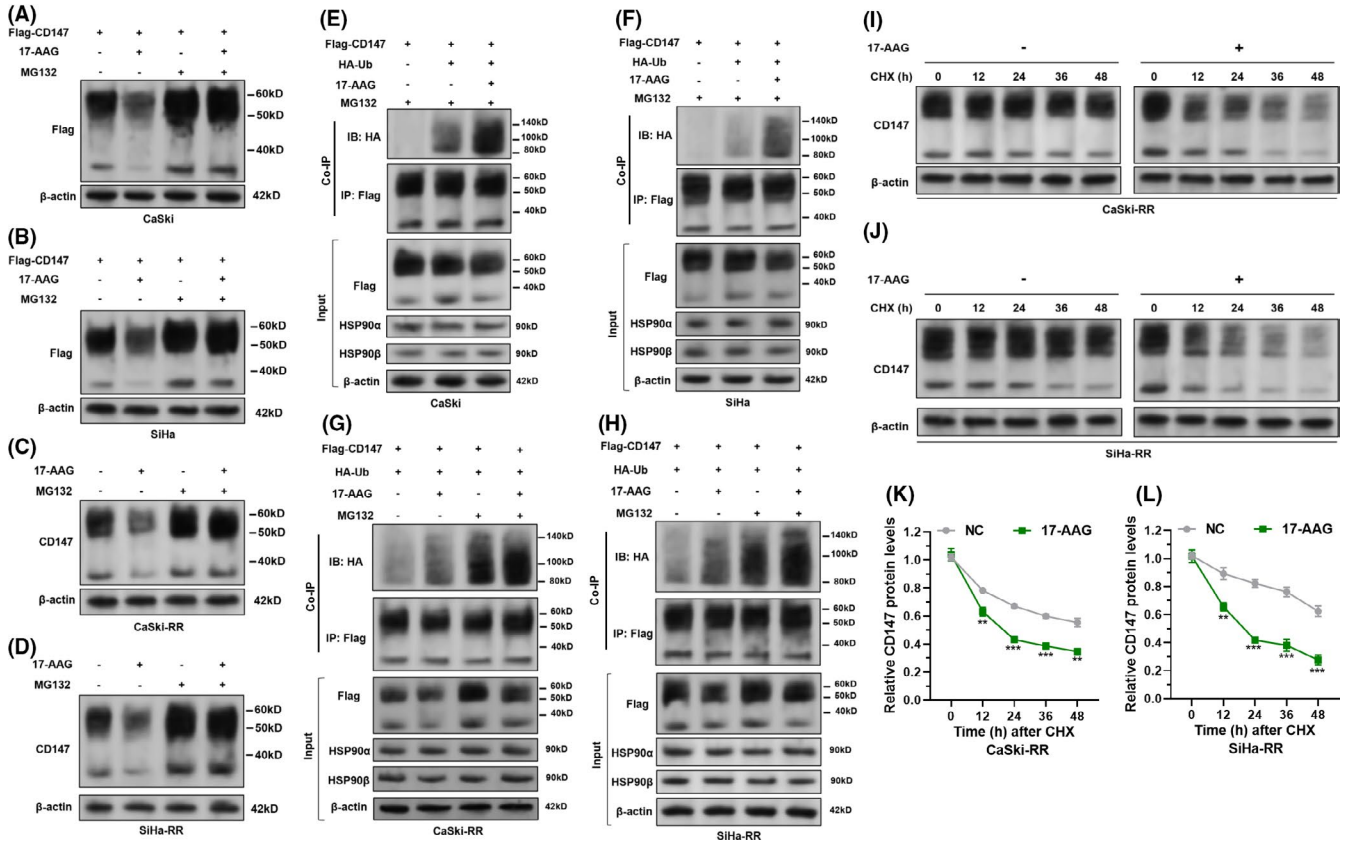

FIGURE 4 Inhibition of HSP90 enhances ubiquitination of CD147 that leads to proteasomal degradation. A, B, Effect of 17-AAG on CD147 proteasomal degradation. CaSki (A) and SiHa (B) cells were infected with lentiviral flag-CD147 for transient overexpression. Then, cells were treated with MG132 (10 μM, 6 h) or control (DMSO) before the addition of 17-AAG (20 nM/24 h for CaSki and 50 nM/24 h for SiHa). Exogenous CD147 levels were detected by western blotting. C, D, CaSki-RR and SiHa-RR cells were treated with or without MG132 (10 μM, 6 h) before adding 17-AAG (20 nM/24 h for CaSki-RR and 50 nM/24 h for SiHa-RR). Then, endogenous CD147 levels were detected by western blotting. E-H, Effect of 17-AAG on CD147 polyubiquitination and proteasomal degradation in CaSki (E), SiHa (F), CaSki-RR (G), and SiHa-RR (H) cells. I-L, CaSki-RR (I, K) and SiHa-RR (J, L) cells were treated with 17-AAG (100 nM for CaSki-RR and or 250 nM for SiHa-RR) or blank control for 4 h, followed by 5 μg/mL CHX treatment for the indicated time. Then, CD147 amount was determined by density analysis (K, L) of western blotting images (I, J). Data are representative of 3 independent biological experiments. Data are reported as the mean ±SD from 3 technical replicates

reduced the degradation of CD147 and canceled 17-AAG-induced CD147 degradation (Figure 5E-G). Overexpression of FBXO6-WT promoted the degradation of CD147, the effect of which was enhanced by 17-AAG treatment (Figure 5H-J). However, overexpression of FBXO6-MT (p.Y241A and p.W242A), a mutant lacking ubiquitin ligase activity,[25] lessened the degradation of CD147 (Figure 5H-J). In addition, this mutant also counteracted 17-AAG-induced CD147 degradation (Figure 5H-J).

3.6 | FBXO6 degrades CD147, which consequently sensitizes radioresistant cells to IR

As we found that FBXO6 could promote CD147 degradation, we then studied whether it modulated radiosensitivity via CD147. *FBXO6* overexpression significantly increased the sensitivity of CaSki-RR and SiHa-RR cells to IR (2 Gy), the effect of which was enhanced by 17-AAG treatment but was weakened by *CD147* overexpression (Figure 6A-C). Moreover, western blot and immunofluorescence assays *FBXO6* overexpression enhanced IR-induced expression of γ-H2AX and γ-H2AX foci (Figure 6D,E). Similarly, the effect was enhanced by 17-AAG treatment, but was weakened by *CD147* overexpression (Figure 6D,E). Overall, these data indicated that FBXO6 sensitized radioresistant cervical cancer cells to IR predominantly by inducing destabilization of CD147 via proteasomal degradation. Using survival data from TCGA-CESC, we confirmed that patients with high *FBXO6* mRNA expression had significantly better PFS compared with their counterparts with low *FBXO6* expression (Figure 6F). However, this trend was not confirmed in OS (Figure 6G).

4 | DISCUSSION

In this study, we confirmed that HSP90 upregulation at the protein level was associated with enhanced radioresistance of cervical

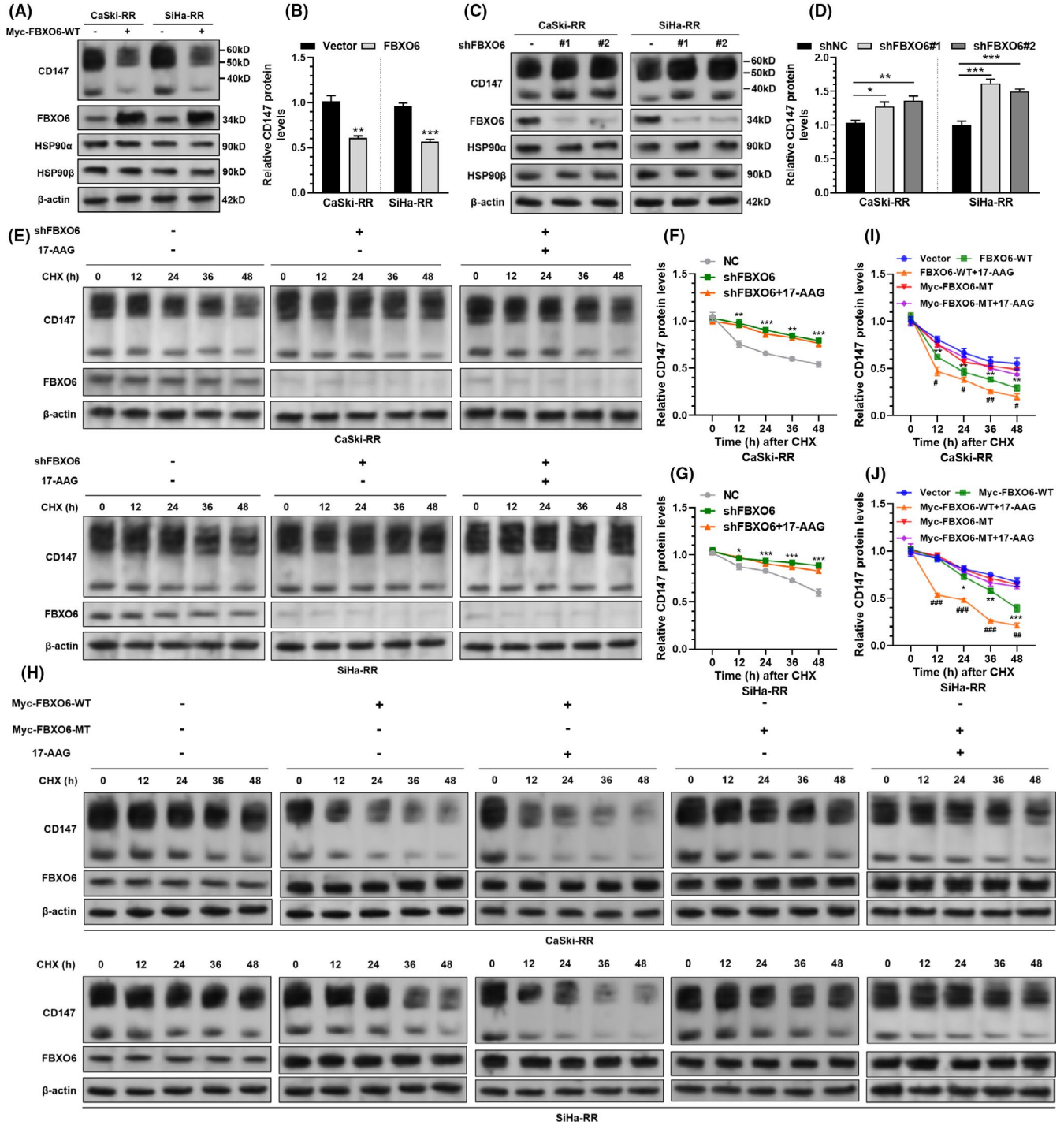

FIGURE 5 FBXO6 ubiquitinates and degrades CD147. A-D, Representative images (A, C) and quantitation (B, D) of the effect of *FBXO6* overexpression (A, B) or knockdown (C, D) on CD147 levels. E-G, CHX was chase assay performed to compare CD147 protein stability in CaSki-RR and SiHa-RR cells after *FBXO6* knockdown, with or without 17-AAG treatment. Cells were infected for transient *FBXO6* knockdown. 48 h later, cells were treated with 17-AAG (100 nM for CaSki-RR and or 250 nM for SiHa-RR) or blank control for 4 h, followed by 5 μg/mL CHX treatment for the indicated time. H-J, CHX was chase assay performed to compare CD147 protein stability in CaSki-RR and SiHa-RR cells with *FBXO6* overexpression (FBXO6-WT or FBXO6-MT) alone or in combination with 17-AAG treatment. Cells were first infected for transient *FBXO6* overexpression. At 48 h later, cells were treated with 17-AAG (100 nM for CaSki-RR and or 250 nM for SiHa-RR) or blank control for 4 h, followed by 5 μg/mL CHX treatment for the indicated time. CD147 amount was determined by density analysis (F, G, I, J) of western blotting images (E, H). Data are representative of 3 independent biological experiments. Data were reported as the mean ±SD from 3 technical replicates

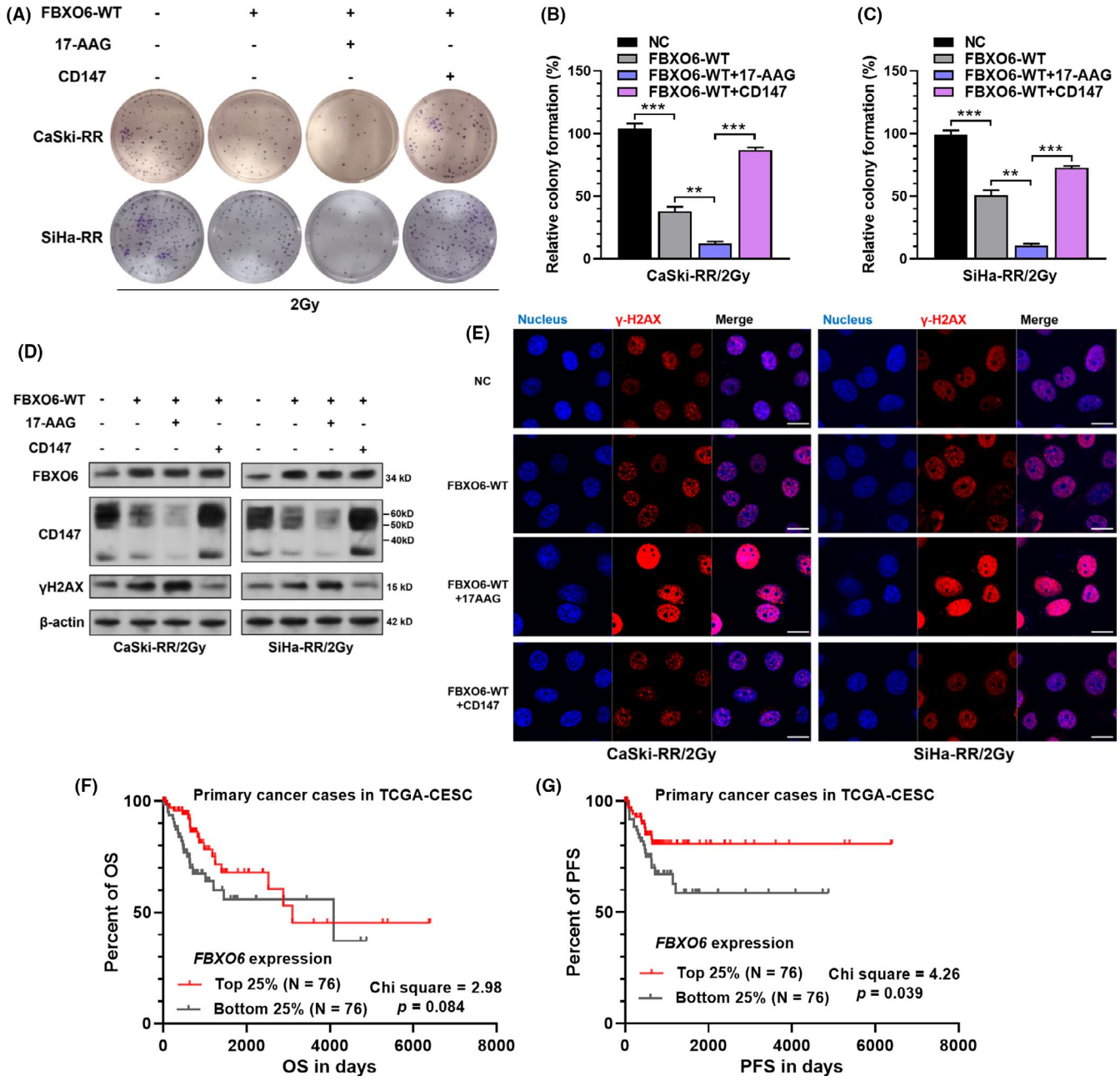

FIGURE 6 FBXO6 degrades CD147, which consequently sensitizes radioresistant cells to IR. A-C, Representative images (A) and quantitation (B, C) of clonogenic assay to examine the effects of X-ray IR (2 Gy) on the growth of CaSki-RR with SiHa-RR cells with transient *FBXO6* overexpression alone or in combination with 17-AAG pre-treatment (20 nM/24 h for CaSki-RR and 50 nM/24 h for SiHa-RR) or *CD147* overexpression. D, Western blotting assay (D) of FBXO6, γ-H2AX and CD147 expression in cells treated as in panel (A), 10 h after X-ray IR (2 Gy). E, Immunofluorescence assay of γ-H2AX foci formation in cells treated as in panel (A), 6 h after X-ray IR (2 Gy). F, G, K-M, survival analysis was performed to compare the difference in PFS (F) and OS (G) between primary cervical cancer cases with the top 25% and bottom 25% of *FBXO6* mRNA expression. Data are representative of 3 independent biological experiments. Data are reported as the mean ±SD from 3 technical replicates

cancer. Inhibiting HSP90 might be a promising strategy to conquer radioresistance in multiple cancers.[13,26,27] Functionally, HSP90 can enhance the stability and function of conformationally labile proteins after primary folding, thereby modulating the functions of the binding proteins.[8] Via inhibiting HSP90, its binding proteins might have accelerated degradation. For example, WT-EGFR is a client protein of HSP90 in cancer cells. Treatment with HSP90 inhibitors geldanamycin and AT13387 facilitated the degradation of WT-EGFR, thereby sensitizing EGFR-dependent cancer cells to chemotherapy and radiotherapy.[28] Ganetespib, a selective inhibitor of HSP90, can act as a radio-sensitizer by reducing IR-induced HIF-1α upregulation in pancreatic cancer cells.[13] Furthermore, 17-AAG can reduce the binding between Hsp90β and its client protein MAST1 and promote proteasomal degradation of Hsp90β, thereby enhancing cisplatin

sensitivity in human cancers.[29] These mechanisms help explain why HSP90 inhibitors show antitumor activity.[30]

Generally, HSP90 forms a clamp structure after homodimerization, anchored by dimerization of the C terminals. Then, the N-terminal domains act as a jaw, which is responsible for ATP hydrolysis and co-chaperones binding.[31] Co-chaperones (such as CDC37, FKBP51, and TAH1) may help to recruit certain client proteins to HSP90 and contribute to regulating HSP90 conformational switch by inhibiting or enhancing ATP hydrolysis.[7] These structural features determined that HSP90 has different client proteins under different conditions. By performing IP and LC-MS/MS in combination, we found that HSP90 interacted with CD147 and FBXO6. CD147 (also known as EMMPRIN or Basigin) is a ubiquitously expressed glycoprotein that is commonly overexpressed in a series of tumors and participates in cancer development.[32] The N-terminal domain of CD147 has 3 glycosylation sites. Therefore, CD147 has non-glycosylated, low-glycosylated, and high-glycosylated forms, ranging from 27 kDa to ~65 kDa.[33,34] High-glycosylated CD147 (ranging from 46 to 65 kDa) is the mature and active form on the transmembrane, with a long-term half-life.[35-37] Previous studies confirmed that CD147 upregulation contributed to enhanced cell proliferation[33] and reduced the chemosensitivity[38] and radiosensitivity[39] of cervical cancer. In this study, we confirmed that 17-AAG treatment decreased CD147 expression, but had little influence on FBXO6 expression. In addition, 17-AAG-induced radio-sensitizing effects were partly abrogated by *CD147* overexpression both in vitro and in vivo. These findings suggested that HSP90 inhibitor 17-AAG exerted radio-sensitizing effects partly by reducing CD147 protein levels in cervical cancer cells.

FBXO6 is a critical substrate adapter of the evolutionarily SCF complex that mediates the ubiquitination of glycoproteins.[25] Its F-box associated (FBA) domains are required for glycoprotein recognition.[40] By performing CHX chase assays, we confirmed that FBXO6 could mediate CD147 degradation via the proteasomal pathway, the effect of which was enhanced by 17-AAG treatment. Therefore, we inferred that HSP90 can enhance CD147 stability by reducing FBXO6-mediated proteasomal degradation. The role of FBXO6 is paradoxical in cancers. In non–small-cell lung cancer, it decreases expression and phosphorylation of Chk1, thereby increasing the sensitivity of the cancer cells to cisplatin-based chemotherapy.[41] However, FBXO6 promoted ovarian cancer cell proliferation, migration, and invasion partially by inducing RNASET2 degradation.[42] Therefore, FBXO6 might have cancer-specific functions, depending on its downstream substrates. In the current study, we further explored the effect of FBXO6 on the radiosensitivity of radioresistant cervical cancer cells. Results showed that enforced *FBXO6* overexpression sensitized CaSki-RR and SiHa-RR cells to IR. These effects were enhanced by 17-AAG treatment, but were weakened by *CD147* overexpression. Survival analysis further confirmed the association between high *FBXO6* expression and favorable PFS among patients with cervical cancer.

Although FBXO6 was identified as a functional E3 ubiquitin ligase facilitating CD147 degradation, the specific binding site and the type of ubiquitination chain remain unexplored. Traditionally, FBXO6 acts as a substrate recognition component of the SCF component. One recent study found that it interacted with the IAD domain of IFN-regulatory factor 3 (IRF3) through its FBA domain to induce ubiquitination and degradation without the involvement of SCF.[43] Considering the promising radio-sensitizing effects of *FBXO6* overexpression and CD147 inhibition in cervical cancer, it is meaningful to explore the detailed mechanisms of FBXO6-mediated CD147 degradation in the future.

In conclusion, this study found that HSP90 (both HSP90α and HSP90β) bound to FBXO6 and CD147 and reduced FBXO6-mediated CD147 polyubiquitination through the proteasomal pathway, thereby promoting radioresistance of cervical cancer cells. These mechanisms further explain why the HSP90 inhibitor exerts radio-sensitizing effects.

ACKNOWLEDGMENTS

None.

CONFLICTS OF INTEREST

None of the authors have conflicts of interest to declare.

DATA AVAILABILITY STATEMENT

The data that support the findings of this study are available from the corresponding author upon reasonable request.

ORCID

Zejun Lu https://orcid.org/0000-0002-7263-7049

REFERENCES

1. Siegel RL, Miller KD, Jemal A. Cancer statistics, 2020. *CA Cancer J Clin*. 2020;70(1):7-30.
2. de Martel C, Plummer M, Vignat J, Franceschi S. Worldwide burden of cancer attributable to HPV by site, country and HPV type. *Int J Cancer*. 2017;141(4):664-670.
3. Shah SC, Kayamba V, Peek RM Jr, Heimburger D. Cancer control in low- and middle-income countries: is it time to consider screening? *J Glob Oncol*. 2019;5:1-8.
4. Chino J, Annunziata CM, Beriwal S, et al. Radiation therapy for cervical cancer: executive summary of an ASTRO clinical practice guideline. *Pract Radiat Oncol*. 2020;10(4):220-234.
5. Tyagi A, Vishnoi K, Kaur H, et al. Cervical cancer stem cells manifest radioresistance: Association with upregulated AP-1 activity. *Sci Rep*. 2017;7(1):4781.
6. Li Q, Wei X, Zhou ZW, et al. GADD45alpha sensitizes cervical cancer cells to radiotherapy via increasing cytoplasmic APE1 level. *Cell Death Dis*. 2018;9(5):524.
7. Li L, Wang L, You QD, Xu XL. Heat shock protein 90 inhibitors: an update on achievements, challenges, and future directions. *J Med Chem*. 2020;63(5):1798-1822.
8. Hoter A, El-Sabban ME, Naim HY. The HSP90 family: structure, regulation, function, and implications in health and disease. *Int J Mol Sci*. 2018;19(9).
9. Johnson JL. Evolution and function of diverse Hsp90 homologs and cochaperone proteins. *Biochim Biophys Acta*. 2012;1823(3):607-613.
10. Garcia-Carbonero R, Carnero A, Paz-Ares L. Inhibition of HSP90 molecular chaperones: moving into the clinic. *Lancet Oncol*. 2013;14(9):e358-369.

11. Kim WY, Oh SH, Woo JK, Hong WK, Lee HY. Targeting heat shock protein 90 overrides the resistance of lung cancer cells by blocking radiation-induced stabilization of hypoxia-inducible factor-1alpha. *Cancer Res*. 2009;69(4):1624-1632.
12. Ernst A, Anders H, Kapfhammer H, et al. HSP90 inhibition as a means of radiosensitizing resistant, aggressive soft tissue sarcomas. *Cancer Lett*. 2015;365(2):211-222.
13. Nagaraju GP, Zakka KM, Landry JC, Shaib WL, Lesinski GB, El-Rayes BF. Inhibition of HSP90 overcomes resistance to chemotherapy and radiotherapy in pancreatic cancer. *Int J Cancer*. 2019;145(6):1529-1537.
14. Nakajima A, Endo H, Okuyama H, et al. Radiation sensitivity assay with a panel of patient-derived spheroids of small cell carcinoma of the cervix. *Int J Cancer*. 2015;136(12):2949-2960.
15. Ij M, van Oorschot B, Oei AL, et al. Enhancement of radiation effectiveness in cervical cancer cells by combining ionizing radiation with hyperthermia and molecular targeting agents. *Int J Mol Sci*. 2018;19(8).
16. Goldman MJ, Craft B, Hastie M, et al. Visualizing and interpreting cancer genomics data via the Xena platform. *Nat Biotechnol*. 2020;38(6):675-678.
17. Lee YY, Cho YJ, Shin SW, et al. Anti-tumor effects of wee1 kinase inhibitor with radiotherapy in human cervical cancer. *Sci Rep*. 2019;9(1):15394.
18. Zhang X, Komaki R, Wang L, Fang B, Chang JY. Treatment of radioresistant stem-like esophageal cancer cells by an apoptotic gene-armed, telomerase-specific oncolytic adenovirus. *Clin Cancer Res*. 2008;14(9):2813-2823.
19. Kim KH, Lee SY, Hwang H, et al. Direct monitoring of fucosylated glycopeptides of alpha-fetoprotein in human serum for early hepatocellular carcinoma by liquid chromatography-tandem mass spectrometry with immunoprecipitation. *Proteomics Clin Appl*. 2018;12(6):e1800062.
20. Bodgi L, Foray N. The nucleo-shuttling of the ATM protein as a basis for a novel theory of radiation response: resolution of the linear-quadratic model. *Int J Radiat Biol*. 2016;92(3):117-131.
21. Uhlen M, Oksvold P, Fagerberg L, et al. Towards a knowledge-based Human Protein Atlas. *Nat Biotechnol*. 2010;28(12):1248-1250.
22. Biau J, Chautard E, Verrelle P, Dutreix M. Altering DNA repair to improve radiation therapy: specific and multiple pathway targeting. *Front Oncol*. 2019;9:1009.
23. Bisht KS, Bradbury CM, Mattson D, et al. Geldanamycin and 17-allylamino-17-demethoxygeldanamycin potentiate the in vitro and in vivo radiation response of cervical tumor cells via the heat shock protein 90-mediated intracellular signaling and cytotoxicity. *Cancer Res*. 2003;63(24):8984-8995.
24. Chen X, Duan LH, Luo PC, et al. FBXO6-mediated ubiquitination and degradation of Ero1L inhibits endoplasmic reticulum stress-induced apoptosis. *Cell Physiol Biochem*. 2016;39(6):2501-2508.
25. Liu B, Zheng Y, Wang TD, et al. Proteomic identification of common SCF ubiquitin ligase FBXO6-interacting glycoproteins in three kinds of cells. *J Proteome Res*. 2012;11(3):1773-1781.
26. He S, Smith DL, Sequeira M, Sang J, Bates RC, Proia DA. The HSP90 inhibitor ganetespib has chemosensitizer and radiosensitizer activity in colorectal cancer. *Invest New Drugs*. 2014;32(4):577-586.
27. Lauber K, Brix N, Ernst A, et al. Targeting the heat shock response in combination with radiotherapy: Sensitizing cancer cells to irradiation-induced cell death and heating up their immunogenicity. *Cancer Lett*. 2015;368(2):209-229.
28. Ahsan A, Ramanand SG, Whitehead C, et al. Wild-type EGFR is stabilized by direct interaction with HSP90 in cancer cells and tumors. *Neoplasia*. 2012;14(8):670-677.
29. Pan C, Chun J, Li D, et al. Hsp90B enhances MAST1-mediated cisplatin resistance by protecting MAST1 from proteosomal degradation. *J Clin Invest*. 2019;129(10):4110-4123.
30. Wang Y, Liu H, Diao L, et al. Hsp90 inhibitor ganetespib sensitizes non-small cell lung cancer to radiation but has variable effects with chemoradiation. *Clin Cancer Res*. 2016;22(23):5876-5886.
31. Prodromou C. The 'active life' of Hsp90 complexes. *Biochim Biophys Acta*. 2012;1823(3):614-623.
32. Yang H, Chen B. CD147 in ovarian and other cancers. *Int J Gynecol Cancer*. 2013;23(1):2-8.
33. Wu Y, Zhou X, Zheng PS. Involvement of CD147 isoform4 in the proliferation of SiHa cells: a possible molecular mechanism of cervical cancer. *Oncol Rep*. 2011;26(3):717-724.
34. Eichner R, Heider M, Fernandez-Saiz V, et al. Immunomodulatory drugs disrupt the cereblon-CD147-MCT1 axis to exert antitumor activity and teratogenicity. *Nat Med*. 2016;22(7):735-743.
35. Bai Y, Huang W, Ma LT, Jiang JL, Chen ZN. Importance of N-glycosylation on CD147 for its biological functions. *Int J Mol Sci*. 2014;15(4):6356-6377.
36. Tian X, Dai S, Sun J, et al. F-box protein FBXO22 mediates polyubiquitination and degradation of KLF4 to promote hepatocellular carcinoma progression. *Oncotarget*. 2015;6(26):22767-22775.
37. Min X, Zhang X, Li Y, et al. HSPA12A unstabilizes CD147 to inhibit lactate export and migration in human renal cell carcinoma. *Theranostics*. 2020;10(19):8573-8590.
38. Zhang F, Zeng YL, Zhang XG, Chen WJ, Yang R, Li SJ. RNA interference targeting extracellular matrix metalloproteinase inducer (CD147) inhibits growth and increases chemosensitivity in human cervical cancer cells. *Eur J Gynaecol Oncol*. 2013;34(5):429-435.
39. Ju X, Liang S, Zhu J, Ke G, Wen H, Wu X. Extracellular matrix metalloproteinase inducer (CD147/BSG/EMMPRIN)-induced radioresistance in cervical cancer by regulating the percentage of the cells in the G2/m phase of the cell cycle and the repair of DNA Double-strand Breaks (DSBs). *Am J Transl Res*. 2016;8(6):2498-2511.
40. Mizushima T, Yoshida Y, Kumanomidou T, et al. Structural basis for the selection of glycosylated substrates by SCF(Fbs1) ubiquitin ligase. *Proc Natl Acad Sci U S A*. 2007;104(14):5777-5781.
41. Cai L, Li J, Zhao J, et al. Fbxo6 confers drug-sensitization to cisplatin via inhibiting the activation of Chk1 in non-small cell lung cancer. *FEBS Lett*. 2019;593(14):1827-1836.
42. Ji M, Zhao Z, Li Y, et al. FBXO6-mediated RNASET2 ubiquitination and degradation governs the development of ovarian cancer. *Cell Death Dis*. 2021;12(4):317.
43. Du X, Meng F, Peng D, et al. Noncanonical role of FBXO6 in regulating antiviral immunity. *J Immunol*. 2019;203(4):1012-1020.

SUPPORTING INFORMATION

Additional supporting information may be found in the online version of the article at the publisher's website.

How to cite this article: Song Q, Wen J, Li W, et al. HSP90 promotes radioresistance of cervical cancer cells via reducing FBXO6-mediated CD147 polyubiquitination. *Cancer Sci*. 2022;113:1463–1474. doi:10.1111/cas.15269